energies

Article

Experimental Study on Bearing Characteristics of Multi-Strata Anchorage System

Yanpei An [1], Nong Zhang [1,2,*], Yiming Zhao [1], Weiwei Wang [1] and Feng Guo [1]

[1] Key Laboratory of Deep Coal Resource Mining, Ministry of Education of China, School of Mines, China University of Mining and Technology, Xuzhou 221116, China; anyanpei@cumt.edu.cn (Y.A.); zhaoyiming@cumt.edu.cn (Y.Z.); 15738512165@163.com (W.W.); guo_feng@cumt.edu.cn (F.G.)

[2] Open Laboratory for Large-Scale Scientific Instruments, Jiangsu Normal University, Xuzhou 221116, China

* Correspondence: zhangnong@cumt.edu.cn

Abstract: One of the important factors affecting the anchoring force of the end encapsulated bolt is the mechanical properties of the rock formation at the anchoring end. For the fully encapsulated bolt, its bearing performance is closely related to the mechanical properties of the bolt passing through the rock stratum and its permutation mode. In this study, a series of laboratory pull-out tests of multi-strata anchorage systems was carried out based on an actual engineering background. The bearing performances and failure mechanisms of the multi-strata anchorage system under different anchoring methods and combinations of rock stratum were studied. The evolution law of the axial force and shear stress of the Agent-Rock interface was also analyzed. The test results showed that, for end encapsulation, changes in the mechanical properties of the rock strata at the anchoring end caused differences in bearing capacity, while full-length encapsulation markedly reduced the disparities. The position of the stratum with the highest general interface shear strength affected the mechanical response of the anchoring interface. The progressive failure process of multi-strata anchorage systems was discussed, and suggestions for rock bolt support in coal mine roadways were also proposed.

Keywords: multi-strata; fully encapsulated bolt; pull-out test; anchoring interface

check for updates

Citation: An, Y.; Zhang, N.; Zhao, Y.; Wang, W.; Guo, F. Experimental Study on Bearing Characteristics of Multi-Strata Anchorage System. *Energies* **2022**, *15*, 1581. https://doi.org/10.3390/en15041581

Academic Editor: Manoj Khandelwal

Received: 20 January 2022
Accepted: 19 February 2022
Published: 21 February 2022

Publisher's Note: MDPI stays neutral with regard to jurisdictional claims in published maps and institutional affiliations.

Copyright: © 2022 by the authors. Licensee MDPI, Basel, Switzerland. This article is an open access article distributed under the terms and conditions of the Creative Commons Attribution (CC BY) license (https://creativecommons.org/licenses/by/4.0/).

1. Introduction

Bolt support is the preferred support method for coal mine roadways and an important supporting technology for safe and efficient mining. Research has shown that it is crucial for roadway safety to form an anchorage structure with a certain thickness in the roadway roof through the bolts [1–4]. The stable thick anchorage structure realizes continuous transfer of the stress inside and outside the anchoring area in the rock mass, thus restraining the development of delamination fractures, and effectively controlling the deformation of the surrounding rock.

According to different encapsulation lengths, the bolt anchoring is divided into end encapsulation, lengthened encapsulation, and full-length encapsulation [5]. The former two methods are widely used for roadway support in China's coal mines, while full-length encapsulation is seldom applied. With the increase of high-intensity mining in recent years, China's coal mines are facing increasing impacts from the complex geological environment and strong mining pressure [6–8]. Due to gradual deterioration of engineering conditions, more coal mines have experienced a multitude of problems to support roadways facing difficult conditions, such as large deformation of soft rock roadway, and fatigue failure of surrounding rock [9] under high ground stress from a strong mining roadway. These complex and difficult roadways create higher demands for the anchoring strength of the bolting system, given the sensitivity of surrounding rock deformation, and for the durability of support. It is difficult to meet these demands using the existing end encapsulation method or lengthened encapsulation. For these two methods, the bolts are in a two-point tension state, the bond length is only 1/3 to 1/2 of the length of the bolt, and the bearing capacity of the bolt depends only on the shear strength of the interface between the rock mass at the anchoring end and the agent. Since most of the bolts are not bonded to the rock mass, in the early stage of rock mass deformation, the bolts will deform together with the surrounding rock and cannot respond to the deformation of the surrounding rock in time. For soft rock roadways and strong mining roadways, controlling the initial deformation of the rock mass is important, and the improper use of end and lengthened encapsulation will miss the optimal time for controlling the deformation of surrounding rock. When the bolt is fully encapsulated, the surrounding rock along the length of the bolt is not only supported by the shearing force but also by the lifting force. A resistance to the deformation of the surrounding rock can be generated immediately to prevent the lateral deformation caused by the shearing motion, so the full-length encapsulation technology can better adapt to the unbalanced deformation of the rock mass [10].

In recent years, scholars have carried out numerous research studies on the bolt force transmission mechanism of the fully encapsulated system and the shear stress distribution of the anchoring interface. In terms of theoretical research, scholars have put forward many theoretical models, and have made profound studies on the stress characteristics of the fully encapsulated bolt and the distribution law of interfacial shear stress under tensile load [11–16]. Wang [17] presented a 3D analytical model detailing the load-displacement characteristics of long and short encapsulation as well as their effects on the evaluated load-displacement response. He et al. [18] studied the mechanical constitutive model and different failure modes of the fully encapsulated system by theoretical derivation. In order to determine the enhancement mechanism of full-length grouting on the interfacial strength of the encapsulation body, Wang [19] carried out theoretical derivation for the shear strength of the anchoring interface before and after grouting, and conducted systematic field tests. Chen [20] studied the load transfer behavior of fully grouted rock bolts and used a closed non-linear model to depict the bond-slip behavior of the Bolt-Agent interface. Cui [21] proposed a simplified numerical procedure for the interaction between the fully-grouted bolt and rock mass with consideration of the endplate. Li [22] provided an analytical model of rockbolts' pull-out behavior under constant confining pressure boundary conditions.

In addition, scholars have also studied the mechanical response mechanism of the fully encapsulated system through laboratory tests, numerical simulations and field tests. Chen [23,24] studied the bearing capacity of the encapsulation system under different loading angles, joint intervals, and different concrete strengths, and concluded that the loading angle (tensile shear loading) had little effect on the final load. Zuo [25] studied the failure modes of encapsulation bodies under different borehole diameters through pull-out tests, as well as theoretical and numerical simulations. Aziz [26] studied the influence of drill hole diameter, drill hole length, thickness of anchor ring, installation time, and effect of gloving on the anchoring strength through laboratory tests and field pull-out tests, and argued that an appropriate increase of drilling length enhanced the load transfer capacity of the encapsulation system. Teymen [27] studied the effect pattern of mineral admixtures in the encapsulation agent on the tensile strength of the fully encapsulated system through the pull-out test. Li [28] and Høien [29] classified the removal forms of fully encapsulated bolts into three categories through a series of pull-out tests, and determined the critical encapsulation length of full-length cement mortar bolts. Kılıc [30] conducted about 80 sets of indoor encapsulation body pull-out tests, and concluded that the mechanical properties of the anchor material have a significant effect on the bearing capacity of the encapsulation system. Feng [31] applied cyclic loads to the steel pipe encapsulation system and tested the durability and stability of the fully encapsulated system. Li [32] studied the shear behavior of fully grouted bolts with different bolting angles or grout strengths. Taking rockbolt types, bolt diameters, bolt lengths and bolting angles into consideration, Luga [33] conducted in-situ fully grouted rockbolts pull-out tests to investigate their load bearing capacity. By investigating the effect of steel fiber grout on the bearing performance of anchored specimens through pull-out tests, Du [34] revealed that the steel fiber grout can improve the pull-out strength of the anchored specimens and affect the post-peak bearing characteristics. Li [35] proposed an analytical model capable of reflecting the plastic strain-hardening of rockbolts subjected to large deformation based on direct shear tests on a bolted joint. Saadat [36] proposed the cohesive DEM framework to study the behavior of grout failure and the bolt–grout interface's shear response under the stepwise pull-and-shear test. Teymen [37] obtained the influence pattern of grouting strength on the axial force and shear stress distribution of the fully encapsulated system through the pull-out test of the encapsulation body.

The load distribution of the fully encapsulated bolt is closely related to the mechanical properties of the bolt passing through the roof formation [38]. Under external forces, rock formations with different mechanical properties deform in different ways, resulting in different anchoring force distribution characteristics along the length of the bolt. Affected by coal formation and stratigraphic sedimentary structures, layered rock mass is especially common in the roof of coal mine roadways [39]. The bolting system that controls the deformation of the rock formation through the bedding planes is subjected to complex forces, thus featuring the diversified causes of failure. There is as yet little research on the influence of multilayer rock mass on the bearing capacity of the fully encapsulated system and the distribution of the interfacial shear stress.

In this paper, multi-strata anchoring specimens with different strength combinations are built for pull-out tests, and the influence of multi-strata on the bearing capacity of the fully encapsulated system is analyzed and the key bearing stratum is determined. We have prepared a force-measuring bolt to study the evolution and distribution law on the axial force and shear stress of the Agent-Rock interface. Based on the test results, this paper discusses the progressive failure process of the multi-strata fully encapsulated system, and provides design concepts for the bolt support of the layered roof roadway.

2. Engineering Background and Methods

2.1. Background

Among various bolt support theories, the suspension theory is one of the most widely recognized theories in Chinese coal mines [40], according to which the bolt support is used to make the unstable strata in the lower part of the roof suspended from the upper strata. Because it is intuitive, easy-to-understand and simple in design, the theory has been widely accepted. There is a common cognition among management of Chinese coal mines that the hard rock layer on the roof should be chosen as the anchoring point. Since the anchoring end of the bolt is located in the stable rock layer, even if the lower weak rock layer is broken, separated or even collapsed, the bolt still can firmly hold the loose and broken rock layer, thus reducing safety hazards. Coal miners prefer to anchor the bolts and cables in the hardest rock stratum. Sometimes, however, the hard rock layers are too far above the roof. Excessive pursuit of this practice will result in unreasonable lengths of supporting components, leading to a weakened active support of the bolts and cables and a poor control of the support system.

Xiaotun Coal Mine is located in Bijie City, Guizhou Province, China. Its major mining seam is #6 seam, with an average burial depth of 283 m and an average thickness of 2.4 m. The mining conditions of #6 seams are relatively complex. The lithology of the roadway is mainly fragmented mudstone or argillaceous rock mass, and most of the roadway is affected by mine water inflow. The surrounding rock of the roadway is severely sloughed, weakened, and deformed by water immersion, encumbering its maintenance and control. The typical conditions and support methods of the roadway of Xiaotun Coal Mine are shown in Figure 1. The surrounding rock of the roadway is mostly argillaceous rock with low strength and can be rapidly weakened by water. A layer of limestone occurs on average 8.0 m away from the roadway roof, with high strength and an average uniaxial compressive strength of more than 50 MPa. Therefore, the limestone is used as the anchoring base point of the rock cable, and a rock cable with a length of 9.0 m is selected to ensure that the insertion length of the rock cable into the limestone is not less than 1.0 m.

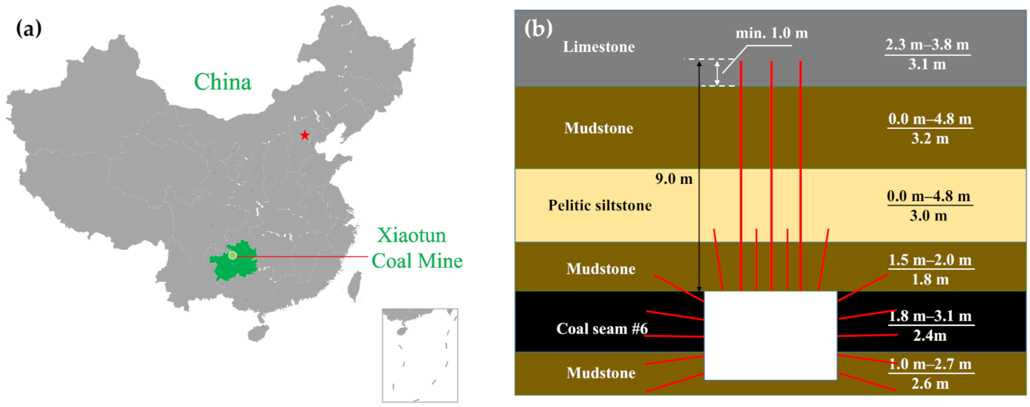

Figure 1. Engineering background: (**a**) location of Xiaotun Coal Mine and (**b**) typical conditions and support methods of the roadway of Xiaotun Coal Mine.

However, the support design of the rock cable has the following problems:

(1) The rock cable is unduly long, and the bolting operation is time-consuming and laborious. The tension force of the rock cable is limited at the field of the coal mine and the corresponding prestress cannot be applied to the rock cable due to its blindly increased length. As a result, the surrounding rock cannot be effectively controlled by the rock cable in a certain range, and the active support effect of the rock cable is weakened.

(2) The suspension range is unduly wide. The rock cable in the limestone provides a large anchoring force, but the weak rock layer in the lower part is too thick. If the control effect is poor, the deformation and damage of the separation layer will gradually accumulate, and the rock cable is under great stress. In this case, the load born by the cable is far beyond the weight of the strata, making it easier for the anchorage system to fail.

The support problems faced by Xiaotun Coal Mine are common in Chinese coal mines. With the bolts and cables together with the surrounding rock forming an anchorage structure, the thickness and strength of the anchorage structure are the keys in controlling the surrounding rock. The thickness of the anchorage structure refers to the effective thickness and is not directly equivalent to the length of the support components. When the same prestress is applied, increasing the length of the bolt and cable will reduce the control effect on the strata within the anchoring range to a certain degree. There is a reasonable range for the length of the bolt and cable. Once the length exceeds the reasonable range, the support effect will be weakened. In this case, the effective thickness of the anchorage structure is actually reduced. Under the premise of ensuring sufficient effective anchoring thickness, how to ensure the bearing capacity of the anchorage system is a problem faced by Xiaotun Coal Mine. The full-length encapsulation technique is one of the solutions to this problem.

The full-length encapsulation technique uses the agent or grouting material to bond together the bolt and the strata within the bolt length. Thus, the fully encapsulated system is more sensitive to the deformation of the strata within the anchoring range, and can immediately generate resistance to the surrounding rock and prevent lateral deformation caused by shear movement, thereby improving the effective thickness and stiffness of the anchorage structure. Unlike end or lengthened encapsulation, the full-length encapsulation does not depend solely on the bonding force on the anchoring interface of the rock strata in the bolt end area. Its bearing capacity correlates to all strata within the encapsulation range. After the system is subjected to the loads, the rock mass in the entire anchoring range will be utilized to bear the loads, and the reliability and safety of the anchorage system are greatly enhanced.

The properties of the surrounding rock are vital to the bearing capacity of the anchorage system. There is a huge gap between the bearing capacities of the anchorage systems with their ends encapsulated in hard rock and in soft rock, respectively. Under these two surrounding rock conditions, even if the full-length encapsulation technology is used, the final bearing capacity and mechanical response of the two systems will still be different. Comparing the bearing capacities and the response characteristics of the Agent-Rock anchoring interface of the two full encapsulation systems is the key task of this paper.

It should be emphasized that the anchorage system in the engineering site is located in a complex mechanical environment, and rock bolts are often subjected to a combination of tensile load, shear load and torsional load. It is difficult for the laboratory to reproduce the real stress state of the rock bolt, and conditions must be simplified. The final results of the tests have certain limitations. In this paper, the pull-out tests of the anchorage system at laboratory scale were carried out by simplifying and simulating the field conditions. Therefore, this paper is devoted to qualitatively analyzing the mechanical properties of the anchorage system and the distribution of the interface shear stress.

2.2. Test Scheme

2.2.1. Determining the Strength of Rock-Like Material

This paper mainly studies the simplified layered rock mass. However, it is extremely difficult to obtain complete natural samples of multi-strata in the field, and other materials must be sought to replace the natural rock. In this paper, a rock-like material made of river sand and cement was used to simulate real rock [41–44]. Upon a series of laboratory tests, the proportion of the rock-like material with strength similar to that of the roof strata of Xiaotun Coal Mine was finally determined, as shown in Table 1. Figure 2 shows the comparison of uniaxial compressive stress-strain curves of the rock-like material and the field rock samples. It was found that the prepared rock-like material and the natural rock samples were similar in peak value of strength, peak position and elastic modulus to a high degree. It means that the prepared specimens are similar in properties to the rock samples obtained in the field, with sound similarity, and can replace the field samples for further in-depth research.

Table 1. Proportion of the rock-like material and its mechanical parameters.

Specimen	Proportion (Cement: Sand: Water)	UCS/MPa	Elastic Modulus /GPa
RM1 (for limestone)	6:1:2	53.5	5.3
RM2 (for politic siltstone)	2:4:1.1	21.9	2.5
RM3 (for mudstone)	1.2:5.6:1	11.4	1.6

2.2.2. Fabrication of Force Measuring Bolt and Calibration of Load Strain

A bolt made of 20MnSi steel by hot rolling was selected, with a diameter of 18 mm and a yield strength of 335 MPa. A tensile test on the bolt was carried out, and the BX120-3AA foil resistance strain gauge was pasted on the bolt to obtain the load-strain relationship of the bolt in the pulling process, as shown in Figure 3. The strain gauges have limitations when they are used to measure the strain of steel, and it is often difficult to obtain the accurate axial force-strain after the test enters the yield stage of the bolt. Therefore, the law of the axial force-strain relationship is obscure in the second half of the curve shown in the figure. The regularity of the elastic stage and the early yield stage was relatively consistent. When the load was applied to the bolt during these two stages, it could be considered that the axial force-strain relationship indicated in the figure was accurate.

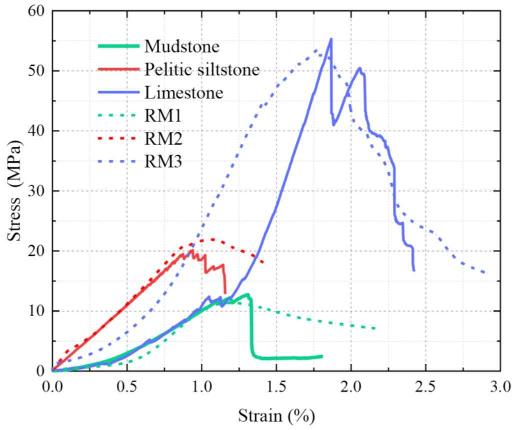

Figure 2. Comparison of uniaxial strength of the rock-like material and that of the field samples.

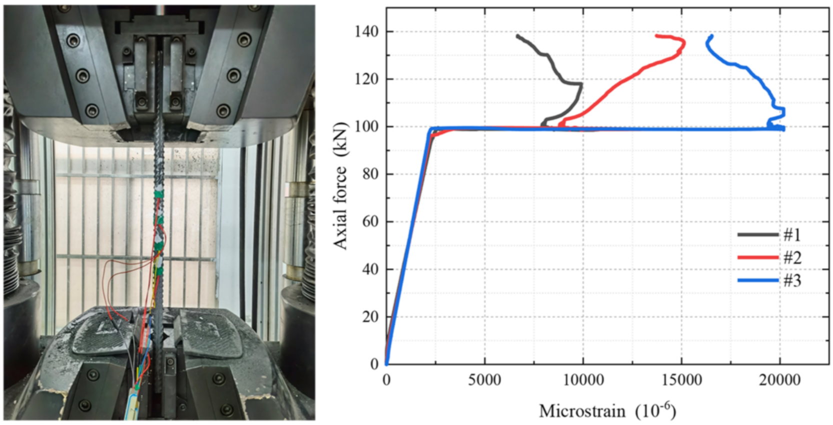

Figure 3. Calibration of load strain of force-measuring bolt.

2.2.3. Preparation of the Specimens

The multi-strata specimens had a size of 200 × 200 × 400 mm, and were poured in three layers, namely Stratum I, Stratum II and Stratum III. The rock layer configuration is shown in Figure 4. Acrylic plates were used to splice a topless cuboid mold for fabricating concrete. When pouring the concrete, a 25 mm PVC pipe was inserted at the center of the mold to be reserved as bolt hole. After each layer of concrete was poured, it was left for 24 h before pouring the next layer. After all the three layers were poured, the specimens were cured for 28 days.

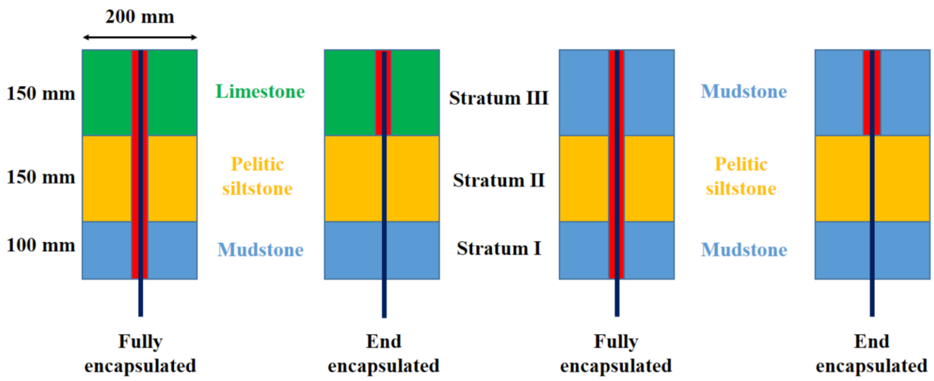

Figure 4. Layout of multi-strata anchorage specimens.

The force-measuring bolt was fabricated, and the strain gauges were arranged as shown in Figure 5. The strain gauges were arranged along both sides of the bolt with an interval of 70 mm. After the strain gauges were pasted, they were sealed with silicone to prevent damage during the anchoring process. The anchoring adhesive was selected to simulate the agent. It was injected into the reserved hole and continuously stirred with a long iron wire to ensure that there were no voids. For the fully encapsulated specimens, the reserved hole was fully filled, and then the force-measuring bolt was slowly screwed into the hole counterclockwise. For the specimens to be encapsulated at the end, the required amount of anchoring adhesive was calculated in advance. After that, the adhesive was quantitatively injected into the reserved hole, and finally the force-measuring bolt was inserted. The number of specimens is shown in Table 2.

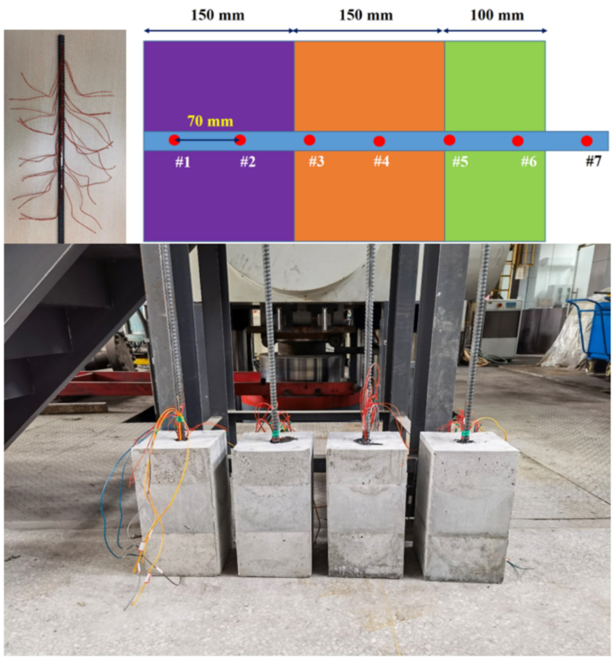

Figure 5. Finished force-measuring bolt and anchorage specimens.

Table 2. Number of specimens.

Specimen	Embedment Length	Stratum III	Specimen	Embedment Length	Stratum III
H-F-1	400 mm	Limestone	S-F-1	400 mm	Mudstone
H-F-2	400 mm	Limestone	S-F-2	400 mm	Mudstone
H-F-3	400 mm	Limestone	S-F-3	400 mm	Mudstone
H-E-1	150 mm	Limestone	S-E-1	150 mm	Mudstone
H-E-2	150 mm	Limestone	S-E-2	150 mm	Mudstone
H-E-3	150 mm	Limestone	S-E-3	150 mm	Mudstone

For the purpose of analysis, the specimens were divided into four categories: hard rock fully encapsulated system (HRFES), soft rock fully encapsulated system (SRFES), hard rock end encapsulation system (HREES) and soft rock end encapsulation system (SREES), according to the rock strength of Stratum III and anchoring method. The term hard/soft rock here refers only to the strength of Stratum III, not the strength throughout the entire specimen.

2.2.4. Test Arrangement

Pull-out tests of the multi-strata anchorage system were conducted, as shown in Figure 6. The LW-100 horizontal pull-out test device for bolt and cable in the State Key Laboratory of Coal Resources and Safe Mining of China University of Mining and Technology was employed as the loading system, which can carry out displacement loading, force loading and cyclic loading on the bolt and the cable. In this test, displacement loading was used, with a loading rate of 1.2 mm/min. A DM-YB1820 dynamic and static strain acquisition instrument was used to monitor the bolt strain. The strain gauges on the bolt were connected with the strain acquisition instrument by 1/4 bridge, with an acquisition frequency of 2 Hz. In this test, a total of eight RS-15A acoustic emission sensors were arranged on the specimens to monitor the acoustic emission events during the test. The acquisition frequency range was 40 k Hz–150 k Hz.

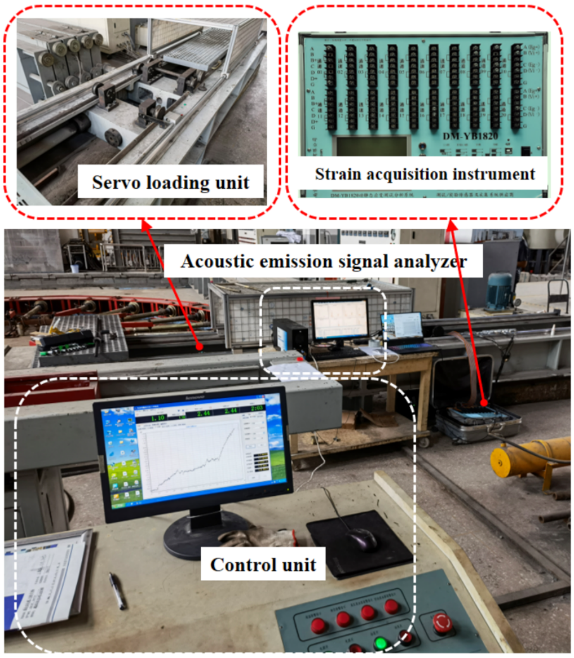

Figure 6. Test equipment and data monitoring devices.

The factor of confining condition cannot be ignored for this test. Whether the confining condition is applied or not directly affects the failure mode and test results of the specimens. If the confining pressure is not applied, it is likely that the specimens may split due to the normal force of the anchorage interface before the specimen reaches the tensile load limit. Therefore, a set of confining pressure applying devices was designed for the test, as shown in Figure 7. The confining pressure applying device was composed of four steel plates, four connecting rods and screws. The four connecting rods were used for the positioning of the screw. The confining pressure was applied on the specimen by tightening the screws on the four sides to press against the steel plates. The amount of the confining pressure was determined by the number of screws at each side and the pre-tightening force applied to each screw. See the following formula for the calculation of the pre-tightening force. A torque wrench was used to apply a pre-tightening torque of 40 N·m to each screw, and the final confining pressure on the specimen was about 2.0 MPa.

$$M_t = KP_0 d \tag{1}$$

where M_t is pre-tightening torque (N·m), K is tightening force coefficient, taken as 0.1–0.3, P_0 is pre-tightening force (N), d is nominal diameter of the thread (m).

Figure 7. Confining pressure applying device.

3. Test Results

3.1. Pull-Out Load

Figure 8 shows the load-displacement curves of the anchorage system under the four conditions. When the anchoring end of the bolt was located in hard rock, the load-displacement curves of fully encapsulation systems and end encapsulation systems were similar. At the same time, it could be seen that the difference in the bearing capacity of the two anchoring methods was small, and their ultimate loads showed almost no difference; the values were 126 kN and 127 kN, respectively. When the tail end of the bolt was in weak rock, the final bearing capacities of the two anchoring methods were significantly different, and were 105 kN and 63 kN, respectively. In terms of post-peak residual strength, SRFES still kept a certain residual strength, which was higher than that of the SREES.

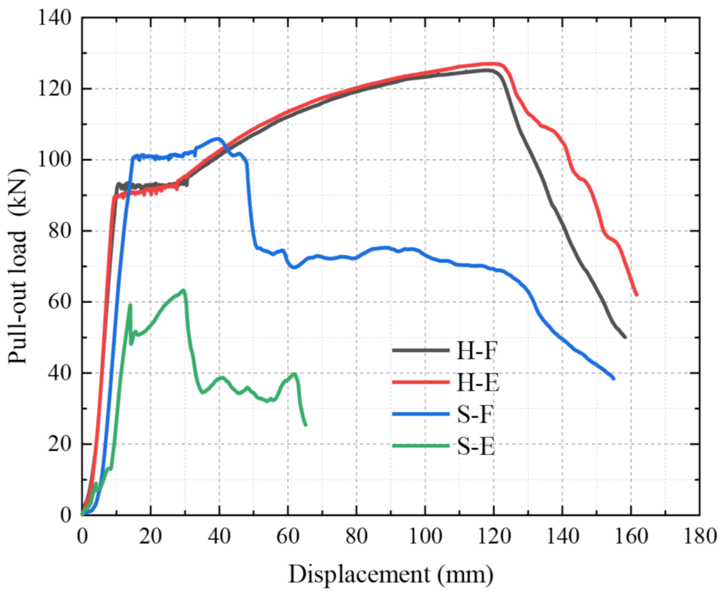

Figure 8. Load-displacement curves of the anchorage systems.

3.2. Axial Force and Shear Stress Distribution

According to the calibrated load-strain value of the bolt in Section 2.2.2, the axial force distribution of the bolt during the pulling process can be obtained. According to Equation (2), the average shear stress value of the anchoring interface between the two strain gauges can be obtained, and the shear stress of this point is taken as the shear stress value at the middle of these two points. Due to the limited range of the strain gauge, only the axial force and shear stress distribution of the bolt within the load of 90 kN load were studied.

$$\tau = \frac{N_i - N_{i+1}}{\pi d \Delta x} \tag{2}$$

where N_i is the axial force (N), d is the bolt diameter (m), Δx is the distance between two strain gauges (m).

3.2.1. Axial Force Distribution

The axial force distribution of the bolt under the four conditions is shown in Figures 9a, 10a, 11a and 12a. With the increase of the load, the axial force distribution of the bolts maintains a consistent trend. The axial force reaches the highest value at the loading end, and gradually decreases after the bolt is deeply inserted into the rock. The axial force borne by Stratum III in the HRFES is commonly low. At this stage, the load is borne mainly by shallow part and has not been transmitted to the deep place. The overall stress on the bolt used for the SRFES is clearly higher than that in HRFES, especially in Stratum III, where the axial force of the bolt changes greatly and the bolt clearly begins to bear the load. With the increase of the load, the curves of the bolts in Stratum I and Stratum II gradually flatten, and their gaps with the pull-out loads become smaller and smaller, indicating that the anchoring interfaces in Stratum I and Stratum II are severely damaged and tend to fail.

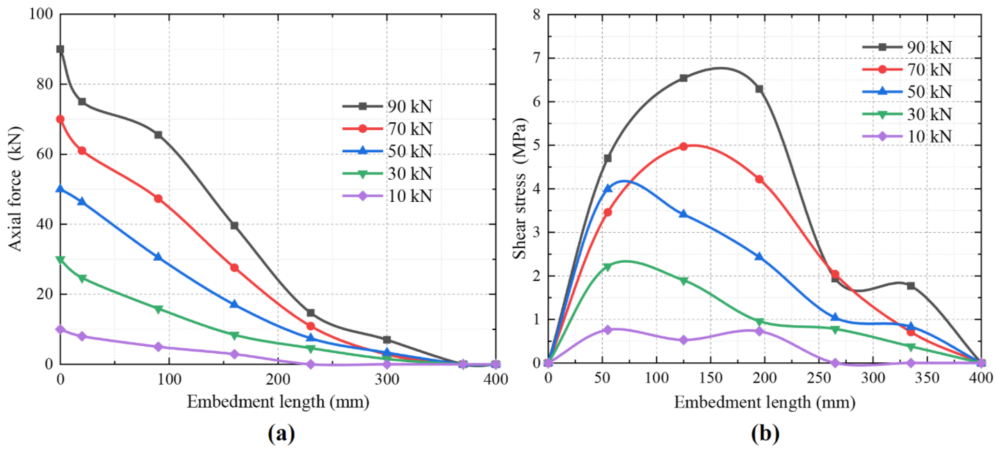

Figure 9. Distribution curve for (**a**) axial force and (**b**) shear stress of the bolt in HRFES.

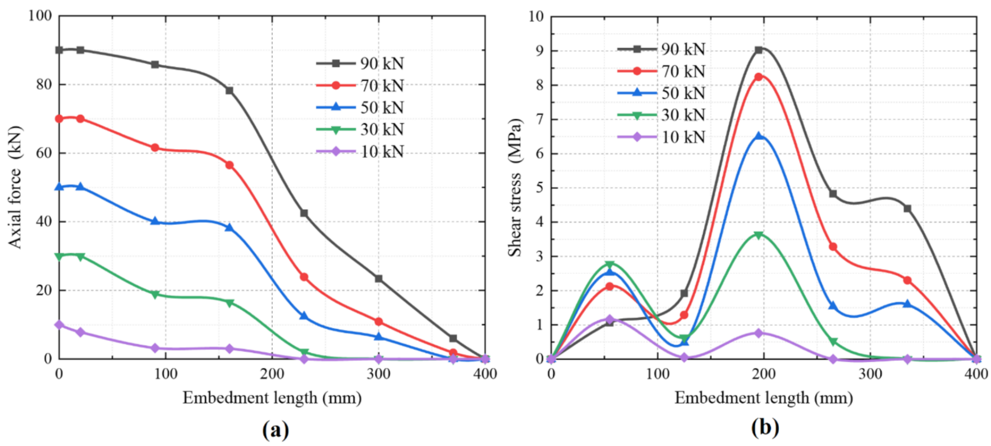

Figure 10. Distribution curve for (**a**) axial force and (**b**) shear stress of the bolt in SRFES.

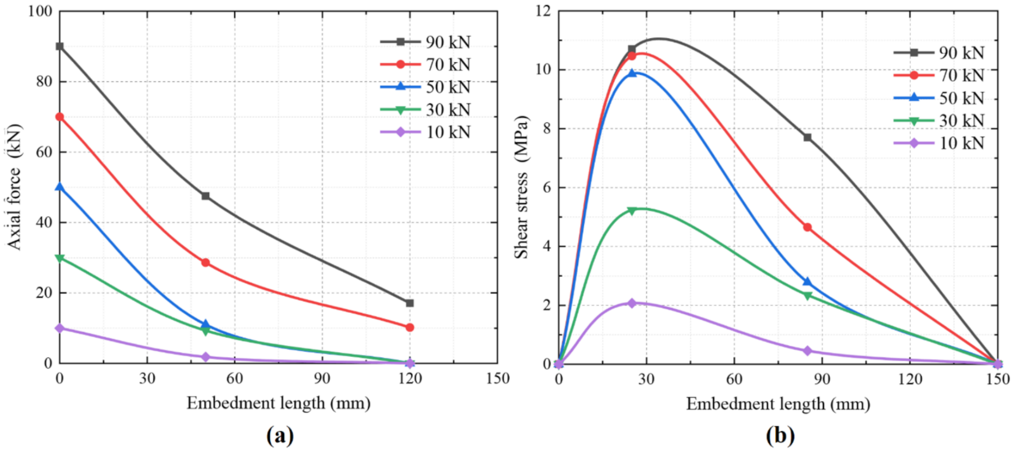

Figure 11. Distribution curve for (**a**) axial force and (**b**) shear stress of the bolt in HREES.

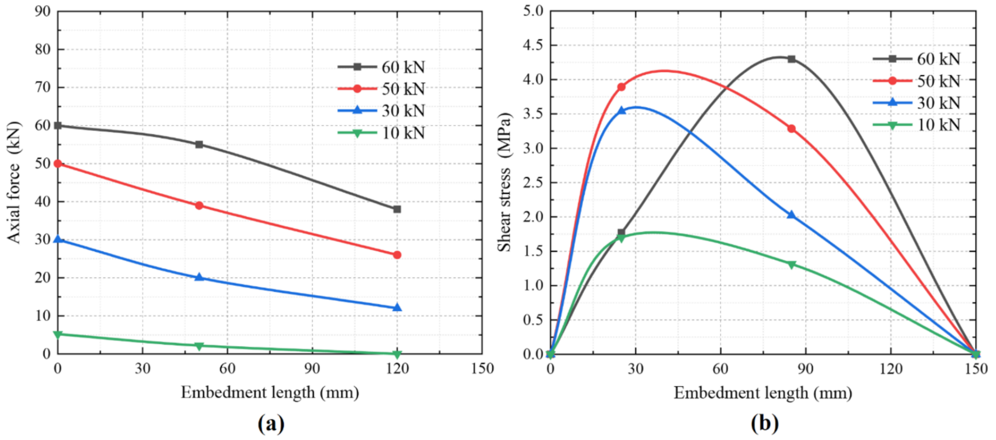

Figure 12. Distribution curve for (**a**) axial force and (**b**) shear stress of the bolt in SREES.

3.2.2. Shear Stress Distribution

See Figures 9b, 10b, 11b and 12b for the shear stress distribution of bolt under four conditions. With the increase of load, the shear stress peak increases gradually, and the peak position moves from shallow to deep parts. However, the movement law differs according to the different strata combinations within the anchoring range.

As for the HRFES, the shear stress is distributed in a single peak pattern, as shown in Figure 9b. When the load is between 10 kN and 50 kN, the peak shear stress appears about 50 mm away from the loading end; when the load is between 70 kN and 90 kN, the peak position of shear stress moves to 150 mm in the deep part. The peak shear stress appears inside Stratum I when the load is lower than 50 kN, which indicates that the shear stress is highly concentrated at the anchoring interface and the damage is ongoing. The peak shear stress moves inside Stratum II when the load reaches 70 kN, which indicates that the interface in Stratum I has failed and entered the post peak stage. Therefore, the peak shear stress goes further into the interior of the rock.

Figure 10b shows the shear stress distribution of SRFES. Viewing from the whole bolt range, its distribution trend shows obvious multi-peak characteristics. When the load is 10 kN, the maximum shear stress within the bolt range appears in Stratum I; it then moves to Stratum II when the load falls between 30 kN and 90 kN. With increase of the load, the anchoring interface of Stratum II becomes the main bearing area. Its first half is in the plasticity stage and bears part of the shear load, and the second half is in the elasticity stage and transfers the load to Stratum III to bear the load together. Therefore, the difference between the axial loads near the strata interface is small, and the shear stress is reduced accordingly. Before reaching the peak load, the pull-out load of the SRFES is jointly borne by the anchoring interfaces of the three strata. The anchoring interface of Stratum II bears the largest part of the shear load, that of Stratum III bears the auxiliary load and that of Stratum I has been seriously damaged.

It can be seen that the shear capacity of the Agent-Rock interface in hard rock is significantly higher than that in soft rock, which also represents the difference in reliability. With the same load conditions and encapsulation length, hard surrounding rock provides stronger shear strength in the anchoring interface and conducts more effective bearing in a smaller range. Under the test conditions, the bearing core is stabilized at the anchoring depth of about 30 mm when HREES is loaded with 70 kN, while the bearing core moves to the anchoring depth of about 90mm when SREES is loaded with 60 kN.

3.3. AE Responses

Figure 13 shows the loads and acoustic emission characteristic curves of the anchorage system under four scenarios, and they have a similar trend. It can be seen that at the initial loading stage, with the rapid increase of load, the debonding failure of the anchoring interface of Stratum I and the small-scale cracks in the rock near the anchoring interface are growing. The acoustic emission phenomenon is relatively intense, and the cumulative count of acoustic emissions increases rapidly with the increase of load. In the yield stage and yield hardening stage, the acoustic emission count increases steadily and slowly until the load reaches the peak. At this moment, the damage on the anchoring interface exceeds the threshold, and it is accompanied by violent acoustic emission. In the post peak stage, the acoustic emission returns to a stable state, and it is mainly generated from the damage accumulation of a small part of the undamaged anchoring interface and the overall slip of the damaged anchoring interface.

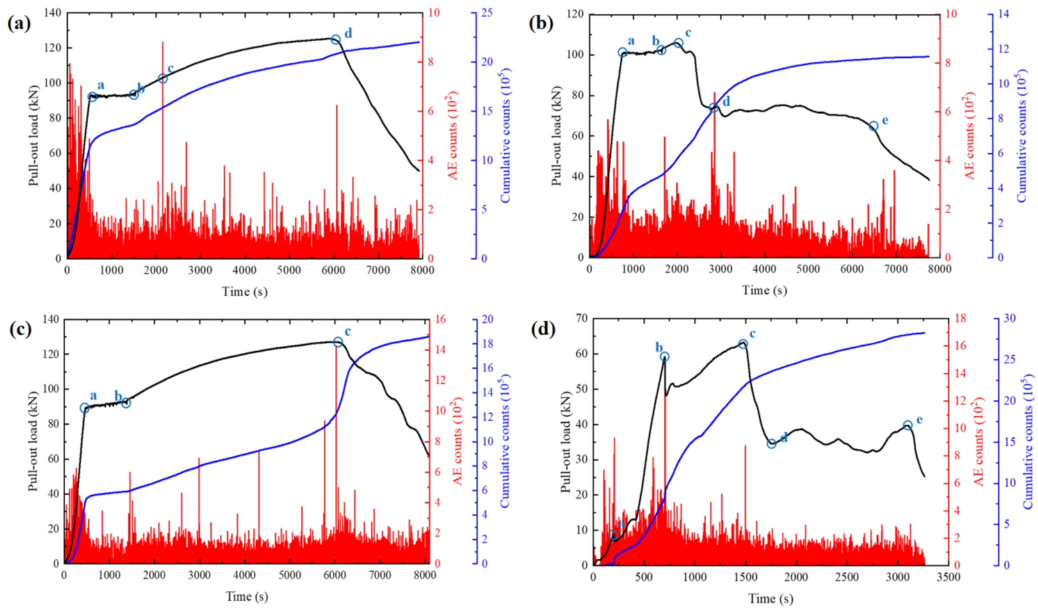

Figure 13. Load and acoustic emission characteristic curve: (**a**) HRFES, (**b**) SRFES, (**c**) HREES and (**d**) SREES.

For the HRFES, there is an obvious acoustic emission at Point c in Figure 13a. It is concluded that the Point c appearance is consistent with the failure time of the bolt strain gauge #4 in Stratum II when it suddenly exceeds the range. Therefore, this point represents the failure and interface debonding of some anchor rings in Stratum II. Active acoustic emission after Point c indicates that the increase of load is accompanied by gradual failure of the anchoring interface at different positions, and the failure gradually moves to Stratum III. The bearing capacity of the anchorage system decreases rapidly when the loading passes over Point d, accompanied by intensive acoustic emission. It indicates that the failure of the anchoring interface has exceeded the threshold, and most parts of the anchoring interface have been debonded and failed, so it cannot bear load any more. At this stage, the acoustic emission sensor in Stratum III can receive more signals than other sensors. It is proved that the key bearing area is located at Stratum III.

For the SRFES, the load in Figure 13b begins to drop rapidly when it reaches Point c. At the same time, the acoustic emission signal becomes active, and the cumulative acoustic emission counts rise rapidly. The closer the sensors are located to Stratum II and Stratum III, the more acoustic emission counts they receive. At the same time, between Point b and Point d, the strain gauges #3 and #4 located in Stratum II gradually exceed the range. It could be concluded from the acoustic emission phenomenon and strain gauge data that the bearing capacity decreases between Point b and Point d are due to the gradual debonding failure of the anchoring interface of Stratum II. Therefore, the bearing area changes to Stratum III. The mechanical properties of Stratum III are weaker than those of Stratum II, and the shear strength and bearing limit of its anchoring interface are also weaker than those of Stratum II. Therefore, it shows a weaker load level than Point c. The anchoring interface between Stratum I and Stratum II has not completely failed, and still has residual bearing capacity and friction shear capacity. Therefore, the anchoring interface of Stratum III does not fail rapidly, but maintains a certain load for a long time.

The load curve of HREES reflects that the end encapsulation system in this stratum is highly reliable, and the third hard stratum is indeed the key to the fully encapsulated system in terms of bearing capacity. In Figure 13d, there are two obvious load drops at Point a and Point b before the load reaches to Peak c in the SREES, both of which are accompanied by violent acoustic emission. The load drop in the loading stage reflects the vulnerability of the anchoring interface in weak strata and the low reliability of the end encapsulation system. It may be noted that the duration of the post peak residual stage of the end encapsulation system in weak strata is very short, and is only about 50% of that of the fully encapsulated system. In the case of weak multi-strata, the fully encapsulated system is much better than the end encapsulation system in terms of pre-peak stability, peak pull-out capacity and post-peak residual capacity. The full-length encapsulation is thus more reliable than end encapsulation.

4. Discussion

4.1. Failure Process of Anchoring Interface in Fully Encapsulated Bolt

According to the analysis of the load transfer behavior and the acoustic emission phenomenon of fully encapsulated bolts during the pull-out tests, we can find that the failure process of the anchoring interface is from shallow to deep. After the axial load increases, the shallow anchoring interface is the first to carry the load, and the dilatation of the anchoring interface is gradually obvious. Before the failure of the shallow anchoring interface, the axial force of rock bolts in this range decreases rapidly with deeper surrounding rock, resulting in a shear stress peak. The location of the peak shear stress at the anchoring interface also represents the main bearing area of the anchorage system. As the axial load increases, the shallow anchoring interface reaches the bearing capacity and then fails in the form of shear and gradually transforms into frictional failure, relying on the frictional effect of the anchoring interface and residual shear dilatation to bear part of the load. In this area, the axial force distribution of the bolt is relatively gentle, and the anchoring interface is damaged and cannot continue to bear higher shear stress, so the peak shear stress is transferred to the more complete anchoring interface in depth. The above process continues during the bearing process of the anchorage system, and the anchoring interface is gradually destroyed from the surface to the inside until the anchorage system fails completely.

The combination of rock strata within the anchorage range also influences the load transfer behavior of fully encapsulated bolts, according to the location of the key bearing stratum. The key bearing stratum is the rock stratum that provides the highest interface shear strength within the bolt length and determines the ultimate pullout load of the anchorage system. Clearly, for the same thickness, a hard rock layer can provide a stronger anchoring interface shear strength than a weak rock layer. Figure 14 shows the localization of acoustic emission events for HRFES and SRFES. It can be seen that the acoustic emission events are mostly concentrated in Stratum I and Stratum II at the early stage of anchorage system bearing, which represents that the main bearing areas of anchoring interface are mostly concentrated here. Before and after reaching the bearing limit of the anchorage system, the acoustic emission events of HRFES are mostly concentrated in Stratum II and Stratum III, while the acoustic emission events of SRFES are mostly concentrated in Stratum II. The distribution of acoustic emission events once again confirms that the key bearing strata for HRFES and SRFES are Stratum III and Stratum II in this test, respectively. The failure of the anchoring interface is gradual, and it is difficult to transfer the load to the deep part if the shallow anchoring interface is intact enough. As shown in Figure 15, when the key bearing stratum is located in the deepest part of the anchorage range, the anchoring interface in the shallow stratum can share part of the load. When the key bearing stratum is located in the middle, the shallow stratum can share the load less; the deeper stratum has difficulty in providing a large contribution to the final load capacity, and can only provide the residual strength after the peak.

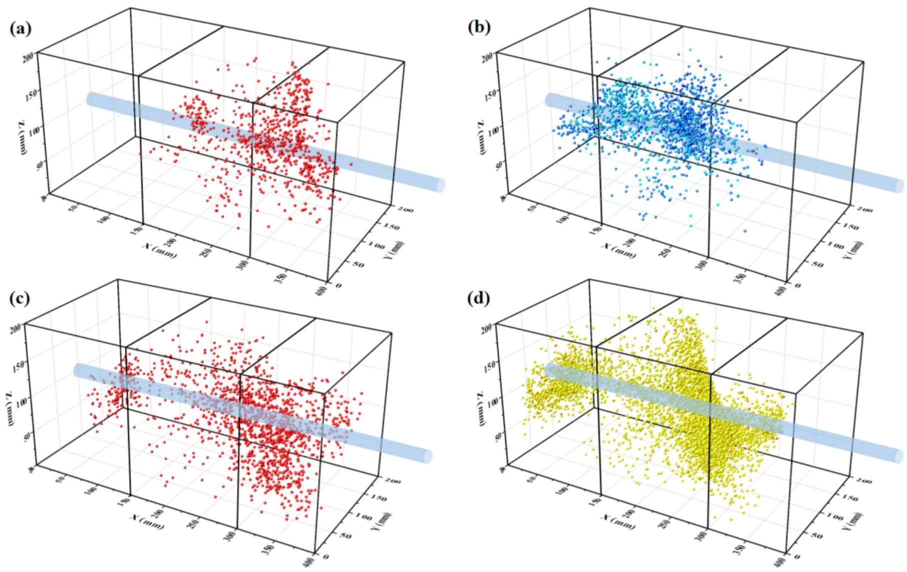

Figure 14. Localization of acoustic emission events: (**a**) HRFES, (**b**) SRFES, (**c**) HREES and (**d**) SREES.

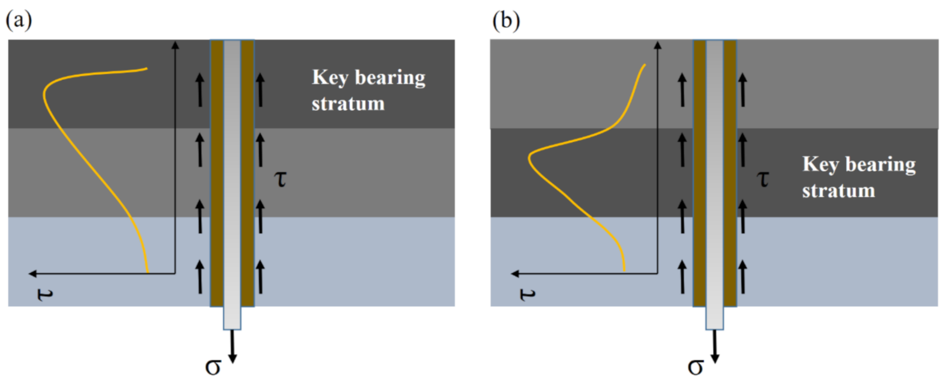

Figure 15. Fully encapsulated bolts with key bearing stratum at different locations: (**a**) deep and (**b**) middle.

4.2. Anchorage Reliability Analysis

The bearing capacity of the anchorage system depends on the shear strength of the anchoring interface, namely the Bolt-Agent interface and Agent-Rock interface. In this test, the Bolt-Agent interface did not fail. It means that, under these test conditions, the shear strength of the Agent-Rock interface is weaker than that of the Bolt-Agent interface. Clearly, the change of the mechanical properties of the surrounding rock has an important impact on the shear strength of the Agent-Rock interface. High rock mass strength and high elastic modulus bring high interface shear strength and high bearing capacity. The peak pull-out load of the anchorage system with the anchoring end located in the hard rock is greater than that of the anchoring end located in the soft rock. As for the end encapsulation, it can be seen that the bearing capacity of the HREES and that in soft rock differs greatly. The former is twice as much as the latter. In the case of full-length encapsulation, the bearing capacity of SRFES is significantly improved, and there is only a 20% gap compared with HRFES. Compared with the end encapsulation, the post-peak bearing strength of SRFES is also significantly improved. It can be seen from Figure 16a that the rock bolt load gradually increases as the shallow rock strata separate or sink due to rock fragmentation, and since the rock bolt is bonded to the full length of the rock stratum, its anchoring interface fails gradually and not abruptly. Even if the shallow anchoring interface fails, the deep interface will continue to carry the load. In contrast, for the end encapsulation shown in Figure 16b, when the shallow deformation accumulates to a certain level, the rock bolt is loaded beyond the anchoring interface bearing limit. After the only anchoring interface fails, the rock bolt will completely lose its supporting function. Therefore, compared with end anchoring, the fully encapsulated bolt increases the safety and reliability of roadway support.

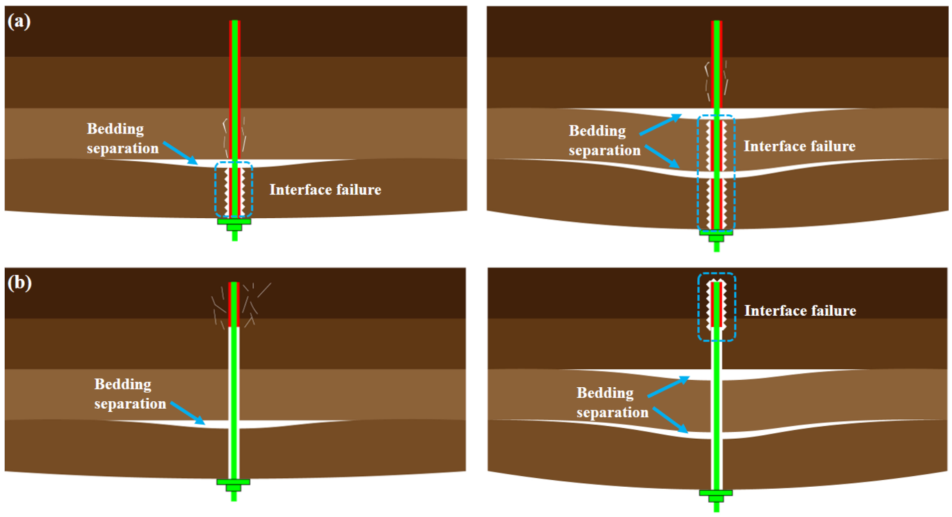

Figure 16. Anchoring interface failure process of (**a**) fully encapsulated bolt and (**b**) end encapsulated bolt.

The reliability of the anchorage system that selects the hard rock stratum as the anchoring base point is significantly higher, whether it is end encapsulation or full-length encapsulation. However, if there is no ideal hard rock stratum as the anchoring point on site, especially when the hard rock stratum is quite deep, blindly increasing the length of bolts and cables to seek the hard rock stratum as the anchoring point will often have the opposite effect. Ground support in coal mines should be considered according to the actual geological conditions, economic benefits and construction difficulty. When there is no hard rock stratum for anchoring, full-length anchorage is a good choice. The fully encapsulated bolt bonds the rock strata within the length of the bolt, which significantly improves the anchoring force. Even if the anchoring point is located in a weak rock stratum, the anchorage system still has high reliability.

5. Conclusions

A series of laboratory pull-out tests of multi-strata anchorage systems were carried out in this study with the anchoring method and the rock stratum strength at the end of the bolt as variables. A novel confining device was designed to ensure that the rock body would not be damaged first during the pullout process, so that the complete mechanical response of the anchorage interface could be obtained, and the reliability of the test results was guaranteed. However, it should be noted that the forces on the anchorage system at the engineering site are extremely complex, and the test only partially represents the site conditions, so limitations of the test results are inevitable. This paper is devoted to qualitatively analyzing the bearing capacity of the multi-strata anchorage system in different rock stratum combinations and the laws of interface failure. We have drawn the following conclusions:

(1) The change of the mechanical properties of the surrounding rock has an important impact on the shear strength of the Agent-Rock interface. Under the end encapsulation condition, the load-bearing performance of the anchorage system in hard rock is much higher than that in soft rock; although the load-bearing performance of the anchorage system in hard rock still surpasses that in the soft rock, full-length encapsulation can significantly reduce the gap of anchoring force between them.

(2) When the fully encapsulated system is subject to a tension load, the axial force of the bolt gradually decreases from shallow to deep, and the peak value of shear stress gradually increases and is transferred to the deeper part. The shear stress distribution of HRFES represents a unimodal pattern, while that of the SRFES looks multimodal, and the shear stress is at a low ebb at the strata interface. We also found that before reaching the ultimate pull-out load, the peak interfacial shear stress of the HRFES located in Stratum III, while the interfacial shear stress peak of the SRFES stopped at Stratum II.

(3) It can be found that in the case of multi-strata, the key bearing stratum of the fully encapsulated system is the rock stratum with the strongest total interfacial shear strength. The location of the key bearing stratum also affects the mechanical response of the anchoring interface. The deeper the location of the key bearing stratum, the more reliable the anchorage system will be. This research finding can provide suggestions for selecting a reasonable bolt length and anchoring method for rock bolt support in coal mine roadways.

Author Contributions: Data curation, Y.A.; formal analysis, Y.A. and Y.Z.; funding acquisition, N.Z.; laboratory testing, Y.A., W.W. and F.G.; writing and editing, Y.A. and N.Z. All authors have read and agreed to the published version of the manuscript.

Funding: This work was financially supported by National Natural Science Foundation of China (52034007) and the Postgraduate Research and Practice Innovation Program of Jiangsu Province (KYCX21_2385).

Institutional Review Board Statement: Not applicable.

Informed Consent Statement: Not applicable.

Data Availability Statement: Data is contained within the article.

Conflicts of Interest: The authors declare no conflict of interest.

References

1. Hou, C.J.; Gou, P.F. Mechanism study on strength enhancement for the rocks surrounding roadway supported by bolt. *Chin. J. Rock Mech. Eng.* **2000**, *3*, 342–345.
2. Zhang, N.; Han, C.L.; Xie, Z.Z. Theory and efficient support technology of continuous beam roof control in coal roadway. *J. Min. Form. Control Eng.* **2019**, *1*, 48–55.
3. Xie, Z.Z.; Zhang, N.; Feng, X.W. Investigation on the evolution and control of surrounding rock fracture under different supporting conditions in deep roadway during excavation period. *Int. J. Rock Mech. Min. Sci.* **2019**, *123*, 104122. [CrossRef]

4. Li, G.; Hu, Y.; Tian, S.M.; Ma, W.B.; Huang, H.L. Analysis of deformation control mechanism of prestressed anchor on jointed soft rock in large cross-section tunnel. *Bull. Eng. Geol. Environ.* **2021**, *80*, 9089–9103. [CrossRef]
5. Kang, H.P.; Cui, Q.L.; Hu, B.; Wu, Z.G. Analysis of Anchorage Properties and Influencing Factors of Resin Bolts. *J. China Coal Soc.* **2014**, *39*, 1–10.
6. Xie, H.P.; Gao, F.; Ju, Y. Research and Exploration of Deep Rock Mass Mechanics. *Chin. J. Rock Mech. Eng.* **2015**, *34*, 2161–2178.
7. Xie, Z.Z.; Zhang, N.; Han, C.L.; An, Y.P. Research on principle and application of cross-boundary anchoring of thick layer of coal roadway roof. *Chin. J. Rock Mech. Eng.* **2021**, *40*, 1195–1208.
8. Gao, M.Z.; Xie, J.; Gao, Y.N.; Wang, W.Y.; Li, C.; Yang, B.G.; Liu, J.J.; Xie, H.P. Mechanical behavior of coal under different mining rates: A case study from laboratory experiments to field testing. *Int. J. Min. Sci. Technol.* **2021**, *31*, 825–841. [CrossRef]
9. Zhu, C.; He, M.C.; Jiang, B.; Qin, X.Z.; Yin, Q.; Zhou, Y. Numerical investigation on the fatigue failure characteristics of water-bearing sandstone under cyclic loading. *J. Mt. Sci.* **2021**, *18*, 3348–3365. [CrossRef]
10. Wu, Y.Z. Research on application of full-length prestressed anchoring strong support system. *Coal Sci. Technol.* **2011**, *39*, 27–30.
11. Cai, Y.; Esaki, T.; Jiang, Y. An analytical model to predict axial load in grouted rock bolt for soft rock tunneling. *Tunn. Undergr. Space Technol.* **2004**, *19*, 607–618. [CrossRef]
12. Ma, S.; Nemcik, J.; Aziz, N. An analytical model of fully grouted rock bolts subjected to tensile load. *Constr. Build. Mater.* **2013**, *49*, 519–526. [CrossRef]
13. Li, D.; Masoumi, H.; Hagan, P.C. Experimental and analytical study on the mechanical behaviour of cable bolts subjected to axial loading and constant normal stiffness. *Int. J. Rock Mech. Min. Sci.* **2019**, *113*, 83–91. [CrossRef]
14. Martín, L.B.; Tijani, M.; Hadj-Hassen, F. Assessment of the bolt-grout interface behaviour of fully grouted rockbolts from laboratory experiments under axial loads. *Int. J. Rock Mech. Min. Sci.* **2013**, *63*, 50–61. [CrossRef]
15. Ma, S.; Zhao, Z.; Nie, W. An analytical model for fully grouted rockbolts with consideration of the pre- and post-yielding behavior. *Rock Mech. Rock Eng.* **2017**, *50*, 3019–3028. [CrossRef]
16. Singh, P.; Spearing, A.J.S. An improved analytical model for the elastic and plastic strain-hardening shear behaviour of fully grouted rockbolts. *Rock Mech. Rock Eng.* **2021**, *54*, 3909–3925. [CrossRef]
17. Wang, Y.J.; Wu, Z.M.; Zheng, J.J. 3D analytical investigation on the overall pullout behavior of grouted anchorages in presence of shear failure of grout. *Eng. Fail. Anal.* **2020**, *109*, 104249. [CrossRef]
18. He, L.; An, X.M.; Zhao, Z.Y. Fully Grouted Rock Bolts: An Analytical Investigation. *Rock Mech. Rock Eng.* **2015**, *48*, 1181–1196. [CrossRef]
19. Wang, Q.; Qin, Q. Study and engineering application on the bolt-grouting reinforcement effect in underground engineering with fractured surrounding rock. *Tunn. Undergr. Space Technol.* **2019**, *84*, 237–247. [CrossRef]
20. Chen, J.H.; He, F.L.; Zhang, S.B. A study of the load transfer behavior of fully grouted rock bolts with analytical modelling. *Int. J. Min. Sci. Technol.* **2020**, *1*, 105–109. [CrossRef]
21. Cui, L.; Sheng, Q.; Dong, Y.; Ruan, B.; Xu, D.D. A quantitative analysis of the effect of end plate of fully-grouted bolts on the global stability of tunnel. *Tunn. Undergr. Space Technol.* **2021**, *114*, 104010. [CrossRef]
22. Li, D.; Li, Y.C.; Chen, J.H.; Masoumi, H. An analytical model for axial performance of rock bolts under constant confining pressure based on continuously yielding criterion. *Tunn. Undergr. Space Technol.* **2021**, *113*, 103955. [CrossRef]
23. Chen, Y. Experimental study and stress analysis of rock bolt anchorage performance. *J. Rock Mech. Geotech. Eng.* **2014**, *6*, 428–437. [CrossRef]
24. Chen, Y.; Li, C.C. Performance of fully encapsulated rebar bolts and D-Bolts under combined pull-and-shear loading. *Tunn. Undergr. Space Technol.* **2015**, *45*, 99–106. [CrossRef]
25. Zuo, J.; Wen, J.; Li, Y. Investigation on the interaction mechanism and failure behavior between bolt and rock-like mass. *Tunn. Undergr. Space Technol.* **2019**, *93*, 103070. [CrossRef]
26. Aziz, N.; Craig, P. Factors influencing the quality of encapsulation in rock bolting. *Rock Mech. Rock Eng.* **2016**, *49*, 3189–3203. [CrossRef]
27. Ahmet, T. Effect of mineral admixture types on the grout strength of fully-grouted rockbolts. *Constr. Build. Mater.* **2017**, *145*, 376–382.
28. Li, C.C.; Kristjansson, G.; Høien, A.H. Critical embedment length and bond strength of fully encapsulated rebar rockbolts. *Tunn. Undergr. Space Technol.* **2016**, *59*, 16–23. [CrossRef]
29. Høien, A.H.; Li, C.C.; Zhang, N. Pull-out and Critical Embedment Length of Grouted Rebar Rock Bolts-Mechanisms When Approaching and Reaching the Ultimate Load. *Rock Mech. Rock Eng.* **2021**, *54*, 1431–1447. [CrossRef]
30. Kılıc, A.; Yasar, E.; Celik, A.G. Effect of grout properties on the pull-out load capacity of fully grouted rock bolt. *Tunn. Undergr. Space Technol.* **2002**, *17*, 355–362. [CrossRef]
31. Feng, X.; Zhang, N.; Yang, S. Mechanical response of fully bonded bolts under cyclic load. *Int. J. Rock Mech. Min. Sci.* **2018**, *109*, 138–154. [CrossRef]
32. Li, Y.Z.; Liu, C.H. Experimental study on the shear behavior of fully grouted bolts. *Constr. Build. Mater.* **2019**, *223*, 1123–1134. [CrossRef]
33. Erion, L.; Erion, P. A pioneer in-situ investigation on the bearing capacity and failure causes of real scale fully grouted rockbolts. *Constr. Build. Mater.* **2021**, *310*, 124826.

34. Du, Y.L.; Feng, G.R.; Kang, H.P.; Zhang, Y.J.; Zhang, X.H. Effects of steel fiber grout on the mechanical performance and failure characteristics of fully grouted bolts. *Structures* **2021**, *33*, 1096–1106. [CrossRef]
35. Li, Y.Z.; Tannant, D.D.; Pang, J.J.; Su, G.S. Experimental and analytical investigation of the shear resistance of a rock joint held by a fully-grouted bolt and subject to large deformations. *Transp. Geotech.* **2021**, *31*, 100671. [CrossRef]
36. Saadat, M.; Taheri, A. Effect of Contributing Parameters on the Behaviour of a Bolted Rock Joint Subjected to Combined Pull-and-Shear Loading: A DEM Approach. *Rock Mech. Rock Eng.* **2020**, *53*, 383–409. [CrossRef]
37. Teymen, A.; Kilic, A. Effect of grout strength on the stress distribution (tensile) of fully-grouted rockbolts. *Tunn. Undergr. Space Technol.* **2018**, *77*, 280–287. [CrossRef]
38. Lu, T.K.; Dai, Y.H. The working characteristics of full-length anchor bolts in the layered roof of mining roadway. *Chin. J. Rock Mech. Eng.* **2010**, *29*, 3329–3335.
39. Zhang, N.; Li, G.C.; Kan, J.G. Influence of weak interlayer layer on the roof of coal roadway on the stability of bolt support structure. *Geomechanics* **2011**, *32*, 2753–2758.
40. Panek, L. *Principles of Reinforcing Bedded Mine Roof With Bolts*; US Department of the Interior, Bureau of Mines: Washington, DC, USA, 1956.
41. Wong, R.H.C.; Chau, K.T. Analysis of crack coalescence in rock-like materials containing three flaws—Part I: Experimental approach. *Int. J. Rock Mech. Min. Sci.* **2001**, *38*, 909–924. [CrossRef]
42. Sagong, M.; Bobet, A. Coalescence of multiple flaws in a rock-model material in uniaxial compression. *Int. J. Rock Mech. Min. Sci.* **2002**, *39*, 229–241. [CrossRef]
43. Xin, C.; Zhihong, L.; Xi, P. Deformability characteristics of jointed rock masses under uniaxial compression. *Int. J. Min. Sci. Technol.* **2012**, *22*, 213–221.
44. Yang, X.X.; Jing, H.W.; Tang, C.A. Effect of parallel joint interaction on mechanical behavior of jointed rock mass models. *Int. J. Rock Mech. Min. Sci.* **2017**, *92*, 40–53. [CrossRef]